RSC Applied Polymers

ROYAL SOCIETY OF CHEMISTRY

PAPER

View Article Online
View Journal

Cite this: DOI: 10.1039/d5lp00370a

Engineering protein-based fiber-reinforced pneumatic actuators

Sandra Edward,[a,b] David Wilcoski,[a] Natalie Taylor,[a] Jason Robinson,[a] Bryan Kaehr,[c] Girish Krishnan[d] and Holly M. Golecki*[a]

Soft actuators provide a basis for building robots that can operate in unstructured or extreme environments. Typical pneumatic soft actuators are made from silicone, which lacks biocompatibility and environmental sustainability. Many hydrogel materials have demonstrated compatibility for biomedical and agricultural fields, yet their application in soft robotics remains limited. In this work, we set out to develop a fabrication method to replace synthetic materials with bioderived alternatives and establish the mechanical characterization of their performance. Our design comprises an entirely protein-based pneumatic actuator. Our base material, gelatin, is mechanically functionalized through plasticizer crosslinking and reinforced with silk threads to build biomaterial fiber-reinforced elastomeric enclosures (bioFREEs). In this paper, we investigate the properties of the biomaterial based on material composition, dehydration state, and fiber reinforcement, and find compositions comparable to traditional materials used for soft actuator fabrication. We conduct Raman spectroscopy analysis to understand the material composition and homogeneity of the hydrogel matrix, as well as the nature of the bonds between the silk thread and the hydrogel matrix in the bioFREE composite. We also study actuator pressure and load-bearing capabilities based on dehydration state and material composition. We find that the protein-based bioFREEs withstand maximum internal pressures of ~96.5 kPa, exert contraction ratios of ~17%, and exert blocked forces of almost 30 N when their diameter is 0.5 cm. They have an upper payload-to-weight ratio of ~519. Together, this demonstrates bioFREEs as a suitable biomaterial alternative to silicone FREEs. We also find evidence that the passive strain-limiting gelatin material properties may be tuned based on dehydration state to mimic the strain-stiffening seen in biological materials or to adapt in variable agricultural microenvironments. Finally, we test the durability and repeatability of these FREEs through loaded and unloaded dynamic tests for at least 40 000 cycles with 82.7 kPa inflation pressure without failure. The mechanical characterization and new fabrication technique for bioFREEs in this work explores durable pneumatic actuators as a platform to employ new materials in traditional soft robot systems.

Received 21st November 2025,
Accepted 4th March 2026

DOI: 10.1039/d5lp00370a

rsc.li/rscapplpolym

1. Introduction

Soft robots made from flexible materials exhibit advantages over traditional robots[1,2] such as enhanced adaptability to extreme environments,[3] safe interaction with humans,[4] and manipulation of fragile objects without damage.[5] In the biomedical field, soft robots can mimic the function of the human body by compliance matching and by distributing forces over larger contact areas to prevent tissue damage.[6] In the agricultural field, soft robots are useful in harvesting for the gentle handling of fruits and vegetables without overly complicated or expensive force feedback.[7,8] However, materials widely used to build soft robots are silicone-based, synthetic, and lack the chemical properties to degrade safely in these environments. To date, common material choices for soft actuators have been limited to synthetic siloxanes, polyurethanes, and nylon materials.[9,10]

Despite the inherent benefits of soft robots for biomedical and agricultural applications, material selection remains an open challenge.[11] These synthetic polymers can be limited in long-term biomedical and agricultural applications since they lack biocompatibility. Silicone has been shown to induce fibrosis within the human body.[12] Synthetic polymers like silicone and PTFE also have limited use in agricultural applications since they are not biodegradable, may contaminate natural resources, and cause harm to local species.[13,14] Thus, there

[a]Bioengineering Department, Grainger College of Engineering, University of Illinois Urbana-Champaign, Urbana, IL 61801, USA. E-mail: golecki@illinois.edu
[b]Mechanical Sciences and Engineering Department, Grainger College of Engineering, University of Illinois Urbana-Champaign, Urbana, IL 61801, USA
[c]Sandia National Laboratories, Albuquerque, NM 87106, USA
[d]Industrial Systems and Engineering Department, Grainger College of Engineering, University of Illinois Urbana-Champaign, Urbana, IL 61801, USA

exists a growing demand for biodegradable and biocompatible soft actuators that mimic synthetic analogues to expand applications in variable environments in these fields.[11,15]

Pneumatically powered soft actuators are a widely used and well-characterized class of devices that provide lightweight, flexible actuation.[16,17] Fiber reinforcement on pneumatic actuators increases their mechanical strength,[18] defines their deformation space,[19] and supports a wide range of motion.[19] Fiber-reinforced elastomeric enclosures (FREEs) are a class of pneumatic soft actuators offering controllable contraction and force generation dependent on internal pressurization.[20,21] FREEs have a high power-to-weight ratio, are inexpensive to fabricate, and are safe for human interaction.[22] The actuator body is an elastomeric cylinder wrapped with fiber reinforcements that control the direction and magnitude of deformation during inflation. These fiber reinforcements increase output efficiency compared to simple elastomeric tubes under the same load.[23] The mechanical behaviour of synthetic FREEs is well characterized.[20,22] FREEs have been applied in wearable assistive devices such as an arm sleeve to reduce injury risk and increase carrying capacity while using crutches,[24] and a cable-driven shoulder exoskeleton to reduce joint and muscle loads.[25] FREEs have also been demonstrated in arm manipulators such as the OctArm,[26] and integrated with rigid robots as an end effector for berry picking.[27] The facile and low-cost fabrication of molded FREEs makes these actuators an ideal platform for building and testing biocompatible soft robots. Development of protein-based textiles creates opportunities for protein-based reinforcing solutions.[28]

In this work, we set out to establish a fabrication method and mechanical characterization of a fully protein-based biomaterial FREE actuator (bioFREE). We take steps toward a goal of the soft robotics field, long-term integration of robots with biological systems. Biomaterials are not without challenges when applied in pneumatic robotic systems. Natural biomaterials require crosslinking to withstand the high, pressurized forces to achieve desired actuation. Previously demonstrated crosslinked hydrogel pneumatic actuators can withstand ~103.4 kPa of pressure during inflation.[29] Inflation pressures may be increased by reinforcing hydrogels with fibers that not only add strength to the material but can also be used to structurally program the actuation mode and direction.

Gelatin, made from denatured collagen, is a good candidate material for mass production of centimeter-scale soft robots. This is due to it being a protein-based biopolymer with demonstrated biocompatibility,[30] biodegradability,[31] tunability with stiffness,[32] and fluid absorbance.[33] Gelatin is typically stabilized by common additives such as glycerol, sugar,[34] or citric acid.[31,35–37] This work utilizes a gelatin mixture stabilized by glycerol. Soft robots made from gelatin have been demonstrated for biomedical applications, including as a magnetically actuated, snake-like, drug release robot[38] and as a surface tethered, gelatin, claw-robot for grasping, transportation, and controlled drug release.[39] Gelatin has also been used to build sustainable agricultural soft robots like a pouch for flora and fauna nutrition,[40] and foam-based actuators with self-germination capabilities.[41] An array of gelatin formulations can be easily and inexpensively manufactured and have some demonstrated utility for soft robot design.

While gelatin actuators have been demonstrated,[31,36] there are very few gelatin-fiber composites used for pneumatic actuation.[42–44] In one example, cotton mesh guided gelatin tubes into s-shape and u-shape arms for object picking.[35] Gelatin-based cotton fiber-reinforcement actuators built *via* 3D printing have integrated sensors and omnidirectional movement for sensing and obstacle removal.[45] However, these examples do not provide a characterization of the relationship between contraction, force, and pressure that is central to actuator function and modeling.

Here, we investigate our composite biomaterial for the effects of material composition, dehydration, and fiber reinforcement. We study the viability of the gelatin material in bioFREEs (Fig. 1A) by evaluating the internal pressures and blocked force characteristics, contraction, and cyclic durability. We demonstrate an application of our bioFREEs as a muscle mechanism by combining a contracting bioFREE with a tendon-actuated finger[46] (Fig. 1B). The contracting bioFREE acts as a muscle connected to the silk tendons for finger flexion. This illustrates potential functionality in other biomedical devices such as joint supports or artificial muscles for assistive physical therapy,[47] or variable-pressure or compression wearables.[48]

Additionally, we show an application of bioFREEs as a climbing robot inspired by a worm's peristaltic motion (Fig. 1C). This robot is composed of a series of contracting and elongating bioFREEs that actuate in series, generating peristaltic motion within a tube. In this example, the upper contracting bioFREE inflates to anchor the robot in place. Following this, the elongating bioFREE inflates to extend the body of the soft robotic worm downwards. Finally, the lower contracting

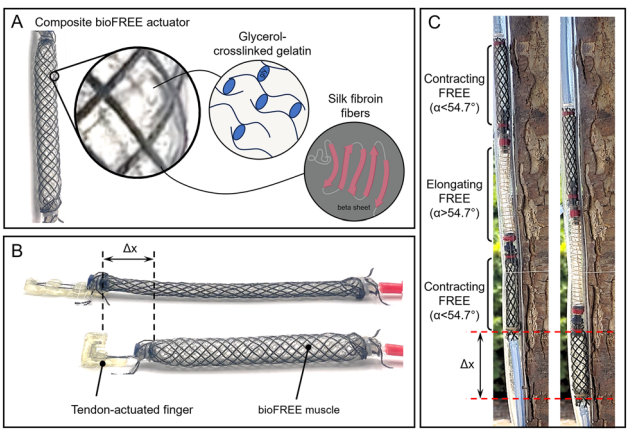

Fig. 1 Protein-based, silk-reinforced gelatin bioFREE actuator. (A) BioFREE actuators are composed of glycerol-crosslinked gelatin wrapped with silk fibroin fibers. (B) Demonstration of a finger-like mechanism made of bioFREE and protein-based tendon actuators. (C) A series of contracting and elongating bioFREEs climbing down a tree using peristaltic motion.

bioFREE contracts and locks the bottom of the actuator in the new position. This sequence is repeated as the actuator climbs down the tube. We envision future applications of bioFREEs in agriculture since its complete protein-based composition may reduce waste and environmental harm if lost or swallowed by wildlife, thus not requiring retrieval. This may enable the use of these FREEs as locomotive worm actuators,[49] burrowing robots to collect soil samples,[50] humidity sensors to measure soil water content through absorption due to the material's hygroscopic property,[51] or as soft actuators for fruit picking with advantages in compliance matching and adhesive surface properties.[27]

Recent advances in soft materials chemistry have demonstrated how engineering materials can enhance mechanical performance and functionality in soft systems for energy and soft matter applications.[52,53] The bioFREE creates added benefits compared to most typical soft pneumatic robots in literature that are either fiber-reinforced but synthetic,[25,27] or non-synthetic but are not fiber-reinforced.[31,36,54] Existing biocompatible polymer-fiber composites in actuators otherwise typically rely on material-level stimuli to induce actuation,[55] or are not completely protein-based.[45] In contrast, this paper presents the development of a soft pneumatic actuator that is simultaneously completely protein-based for biocompatibility and sustainability, as well as fiber-reinforced for directional motion control and increased payload-to-weight ratio. We present the design and fabrication of gelatin and silk fibroin bioFREE actuators, followed by mechanical characterization that may inform a new class of soft robot chemistry to replace common synthetic materials.

2. Materials and methods

2.1. Materials

To fabricate bioFREEs, gelatin is crosslinked with glycerol plasticizer to form a stable polymer network.[36] The elastomeric material is made from a mixture of porcine gelatin (Custom Collagen Superclear Gelatin, Addison, IL),[56] laboratory-grade glycerol (Carolina, North Carolina),[57] and piped water. The weight ratios of gelatin, glycerol, and water (gel : glyce : wat) tested were 1 : 2 : 2, 1 : 2 : 4, or 1 : 2 : 8, as previously reported.[35,36] Gelatin and glycerol are mixed in a room at 21 °C and 50% RH. Water heated to 100 °C is added to the solution and stirred until the mixture is completely dissolved (~5 minutes).

2.2. Actuator fabrication

The gelatin material is cast in molds after stirring and before complete cooling. Before pouring, molds are sprayed with a layer of Universal™ Mold Release (Smooth-On, Inc.). The casts cure in 20 min, open to room temperature air at 21 °C and 50% RH. The samples are maintained in a room with constant temperature and relative humidity of 21 °C and 50% RH. These conditions were tested periodically and had minimal variations. For dehydration testing, gelatin sheets (3 cm × 4 cm) are demolded and weighed at regular intervals every 4–8 hours until there is no significant change in weight over three time points. Thus, the specimens were equilibrated at these conditions to a steady mass. For uniaxial tensile testing, crosslinked gelatin is cast in 3D-printed dogbone molds. After 20 min, samples are removed from the mold and dehydrated to a steady mass before testing. To create fiber-reinforced dogbone samples, three strands of biodegradable silk (Michaels, The Beadsmith Silk, size FFF)[58] or cotton fibers (123Stitch)[59] are equidistantly aligned along the long axis of the mold. A second layer of gelatin material is poured and spread into a ~1 mm layer to bind the fibers to the gelatin material. The sample is cooled for 7 min at room temperature, demolded, and dehydrated.

Varying actuation motions of FREE actuators can be achieved by designing fiber reinforcement at specific angles, as previously reported.[20] Fibers restrain the expansion of elastomeric tubes, dependent on fiber angle. Gelatin tubes with no reinforcement expand around 1.5 times more in both the radial and longitudinal directions than the reinforced bioFREEs when pressurized to 41.3 kPa (Fig. 2A). Expansion varies depending on the material and its strain-stiffening and viscoelastic characteristics. When the fiber angle, α, $\beta > 54.74°$ from the long axis, the bioFREE will elongate (Fig. 2B). If α, $\beta < 54.74°$, the bioFREE contracts (Fig. 2C). When the fiber angles are unequal ($\alpha \neq \beta$), the resulting FREE rotates while extending or contracting (Fig. 2D).

To fabricate bioFREE composites, the gelatin mixture described above is poured into a two-piece 3D printed cylindrical mold (height = 25 cm, outer radius = 1.3 cm) designed for FREEs (Fig. 3A). Elastic bands hold the mold closed. A dowel

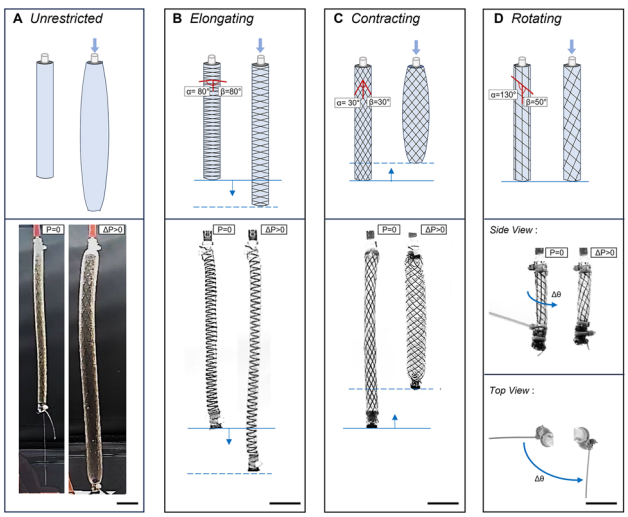

Fig. 2 Actuation motion of bioFREEs based on the threading angle. (A) Inflation of a gelatin tube (no fibers) when pressurized. (B) Elongating motion in the axial direction of the bioFREE with symmetrical fiber angles $\alpha = \beta > 54.74°$. (C) Contracting motion in the axial direction with symmetrical fiber angles $\alpha = \beta < 54.74°$. (D) Rotating motion of the bioFREE with unequal fiber angles ($\alpha \neq \beta$). All actuators are pressurized to 41.3 kPa. All scale bars are 2 cm.

rod (diameter = 0.5 cm) is aligned in the center of the mold to create the hollow through hole of the FREE. The mold and dowel are sprayed with Universal™ Mold Release. The mold has protruding striations along the inner wall that create indentation lines on the cast gelatin material designed for the desired movement. These indents later guide the thread wrapping. Gelatin cures in ~2 hours in the mold. After demolding with a dowel rod in place, the bioFREE dehydrates on wire racks at 21 °C and 50% RH. Fiber threads are wrapped around the indentations aligned in the material. The bioFREEs are then dipped into a gelatin mixture to bind the gelatin and threads, and are again cured for at least ~2 hours before testing. The 1 : 2 : 8 bioFREE samples shrink in length by approximately 17% after 48 hours due to a ~70% weight loss when dehydrated, after which no more weight loss occurs (Fig. 3B). Biologically derived and processed biopolymers are known to have variability from batch to batch. To account for this, all tests were run with samples from three different material batches. Since the fabricated bioFREEs are sensitive to water, weight measurements are taken immediately on demolding, and are subsequently taken every 4–8 hours until the expected dehydration stage has been reached. They can then be conserved in plastic wrap until any experiments are conducted on them within 24 hours. Any water loss during experiments is minimal since most experiments take less than an hour to run. If the bioFREEs are then left alone in the open environment post dehydration and post-experiment, they will advance to the 70% dehydration state and will remain that way until they are disposed of.

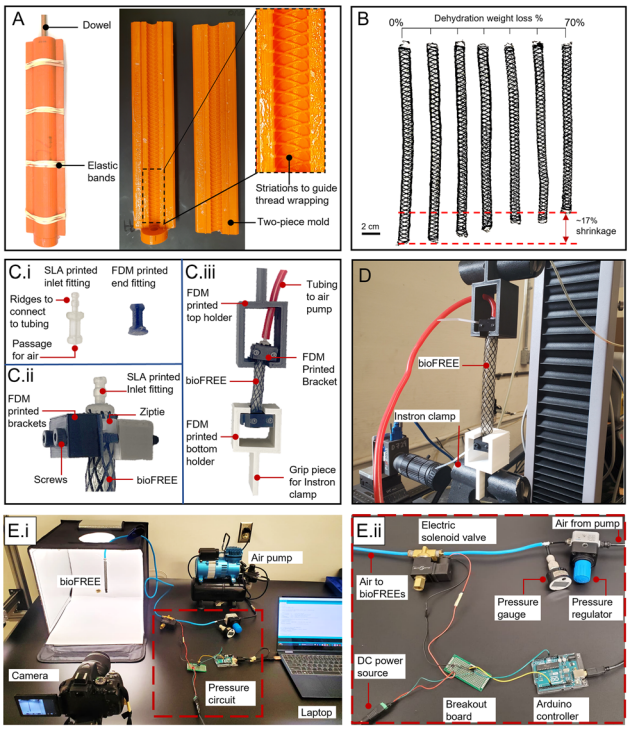

Fig. 3 Fabrication of the gelatin-based bioFREEs. (A) Two-piece mold used to cast the gelatin bioFREEs with a dowel rod to create the cylindrical hollow. (B) Picture of the shrinkage due to dehydration of the 1 : 2 : 8 (gel : gly : wat%) bioFREEs. Scale bar is 1 cm. (C(i)) Custom-designed and printed bioFREE inlet fittings. (C(ii)) Bracket attachment for load testing. (C(iii)) Load testing custom setup. (D) Experimental setup of the bioFREEs with the MTS Criterion for load tests. (E(i)) Experimental setup for displacement cyclic testing. (E(ii)) View of the pressure circuit for cyclic testing.

2.3. Mechanical testing of the gelatin material

For mechanical testing of the bioFREEs, one end of the actuator is fitted with a custom SLA printed inlet fitting with ridges to connect tubing to the actuator (Fig. 3C(i)). The opposite end fitting that seals the bioFREE is FDM printed (Fig. 3C(i)). The inlet and end fittings are secured with zipties. BioFREEs are inflated with the use of an air compressor (Model TC-326T, Master Airbrush).[60] Internal pressure is read with a pressure gauge (EW-68950-30, Cole-Parmer). Uniaxial tensile tests are performed using the MTS CRITERION C43.104E (Eden Prairie, MN) instrument with a 500N load cell. All tensile tests are run at a speed of 0.5 mm/sec until failure. To account for the circular cross-section of the bioFREEs when clamping without compromising the integrity of the air inlet, custom brackets were FDM printed and adjoined to the bioFREE fittings (Fig. 3C(ii)). The BioFREEs fixed with brackets slide into custom FDM printed attachments that were clamped by a Universal Testing Machine for loading (Fig. 3C(iii)).

2.4. Blocked force and force displacement tests

For load testing, this work utilizes the MTS CRITERION C43.104E instrument with a 500 N load cell (Fig. 3D). Blocked force is the axial tensile force exerted by the pressurized bioFREE when its length remains fixed at its undeformed configuration.[61] This experiment is conducted by clamping the bioFREE in place at its initial, unpressurized length and pressurizing the actuator to measure the applied force on the load cell. Force *vs.* negative displacement tests are conducted by pressurizing a bioFREE initially constrained at its undeformed length and then applying fixed intervals of negative displacement to measure the change in the steady state force exerted by the actuator on the load cell.

2.5. Dynamic testing

Actuator contraction response to dynamic pressure is evaluated for bioFREE contraction subject to cyclic pressurization. An Arduino is used to control a three-way valve electric solenoid that can pressurize or vent the bioFREE (Fig. 3E). Videos taken throughout the experiment, and the displacement is tracked over cycles using a modified OpenCV code.[62] The Actuator dynamic loading response is evaluated with the MTS CRITERION C43.104E instrument. The same pressure circuit setup is used with the solenoid switch controls input from the MTS criterion rather than the Arduino. The bioFREE is constrained within the instrument's stationary clamps while a cyclic pressure is applied to it, exerting a cyclic blocked force on the 500 N load cell.

3. Results

3.1. Material characterization

Dehydration of the gelatin material is an important stage in the actuator fabrication process to prevent gelatin tear under applied air pressure. To understand the gelatin composition that creates reliable actuators, we measured dehydrated material behavior based on the initial water content of 1 : 2 : 2, 1 : 2 : 4, and 1 : 2 : 8 (gel : gly : wa wt%) formulations (Fig. 4A). When exposed to air, the material dehydrates and loses water weight, causing the material to shrink. We observed that weight remains stable after 125 hours drying at ambient conditions (RT, 50% RH), *i.e.*, no more net exchange of water occurs with the environment, bringing the gels to sorption equilibrium.[63] The 1 : 2 : 8 material has the highest dehydration rate and loses 70% of its total weight, corresponding to nearly 100% of the water weight initially added when making the material mixture. In comparison, the 1 : 2 : 4 samples lose 45% of their total weight, corresponding to a 78% loss of the water initially added, and the 1 : 2 : 2 samples lose only 20% of their total weight, corresponding to a 50% loss of the water initially added. This reduction in dehydration weight loss and increase in water retention in the 1 : 2 : 2 samples is due to a comparatively higher concentration of hygroscopic glycerol in the mixture. The glycerol binds to water molecules, creating a higher osmotic pressure than pure water, draws water into the material, and effectively retains it.[64–66] Higher dehydration rate of the 1 : 2 : 8 material causes samples to become 2.35 times thinner and have an increased stiffness during tensile loading despite initially containing the highest water content (Fig. 4B). In comparison, the 1 : 2 : 2 and 1 : 2 : 4 samples have lower stiffness (Fig. 4B) with water particles trapped within the material matrix. Evaluating stress–strain plots and generally handlability without tearing lead us to explore the 1 : 2 : 8 formulation further.

We conducted experiments to understand the impact of dehydration level on material stiffness. Sets of 1 : 2 : 8 non-reinforced (−Fib) dogbone samples at dehydration weight loss of ~70% (maximum dehydration amount), 40%, and 30% were uniaxially loaded in tension (Fig. 4C). The material is only at sorption equilibrium at the 70% dehydration level, the 40% and 30% water-loss specimens were tested immediately upon reaching their target mass or stored briefly in plastic wrap to maintain that hydration level until testing. As expected, our data showed a distinct increase in stiffness as the samples dehydrated. A stress–strain curve of Ecoflex™ 00-30 (Smooth-On, Inc.) silicone, a common material used to build synthetic FREE actuators, is also tested.[67,68] While silicone behavior aligns with the 30% dehydrated 1 : 2 : 8 gelatin material, full dehydration of gelatin creates the most robust, workable material. Elastic modulus of the ~70% dehydrated 1 : 2 : 8 material is E = 0.14 MPa, calculated at the intersection of the dashed lines (Fig. 4C), where both transverse and longitudinal strains of the bioFREEs are calculated to be less than 1 *via* image analysis. The effects of the silk fiber reinforced (+Fib) gel-fiber dogbone composites confirm that fiber reinforcement increases stiffness, as expected (Fig. 4D). The gel-fiber composites exhibit the distinctive bimodal, J-shape seen in biological tissues as a natural 'strain-limiting' mechanism, preventing damage from excessive strain.[69] This important property exhibited by biological materials is not observed in synthetic silicones. Thus, gelatin may both serve as a substitute for synthetic materials in FREE actuators and provide additional benefits like this strain-limiting behavior.

Raman spectroscopy was conducted according to the method in section S1 to ensure that the mixed elastomer material (gelatin/glycerol/water) used for the bioFREEs is homogeneous, even at the different dehydration stages of the bioFREEs. Thus, spectra were collected at five locations with a spacing of ~240 μm on cross-sections of the gelatin matrix from the outermost edge to the innermost edge. Fig. S1A shows the spectra for the 70% dehydration sample, and identifies the peaks in the spectra that relate to all three of the material's constituents. We can identify peaks for gelatin as CH_2 at ~3000 cm^{-1}, amide A at 3349, amide I at 1613 cm^{-1}, and amide II at 1554 cm^{-1}, which aligns with the typical gelatin material spectrum.[70] We identify water peaks as the broad OH band at 3500 cm^{-1}.[71] Finally, we also identify glycerol's spectral footprint from 480 cm^{-1} to 1500 cm^{-1} in our matrix mixture.[72,73] It is seen that the peaks overlap among all the spectra, indicating that the 70% dehydrated bioFREE is both chemically and compositionally homogeneous (Fig. S1B). The 0% dehydrated material is chemically homogeneous, but may have slight differences in composition due to active dehydration of water (Fig. S1C).

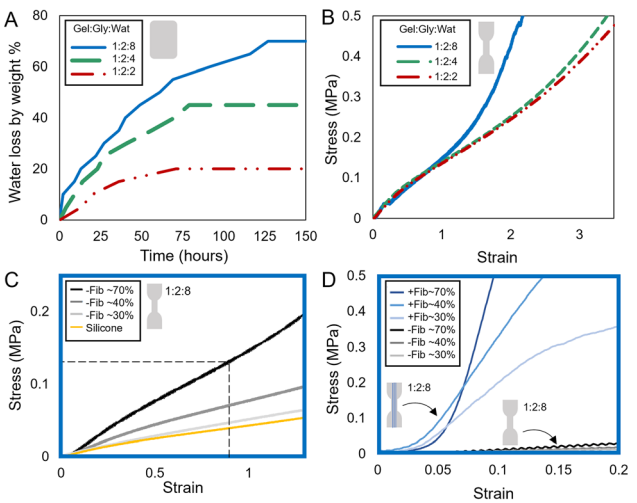

Fig. 4 Material testing at 21 °C and 50% RH. (A) Dehydration of gelatin block samples in terms of weight percent retained after dehydration (n = 3 batches). (B) Instron stress–strain tests of unreinforced gelatin dogbone samples for different material compositions (n = 3 batches). (C) Instron stress–strain test of 1 : 2 : 8 material for no fiber (−Fib) gelatin dogbones at three different stages of dehydration compared to Ecoflex 30 Silicone dogbones (n = 3 batches). (D) Instron stress–strain test of 1 : 2 : 8 material for silk fiber reinforced (+Fib) *vs.* −Fib gelatin samples at three different stages of dehydration, weight loss % (n = 3 batches).

3.2. Pressure capacity of bioFREEs

To understand the nature of the interface between the silk fiber and the gelatin matrix, we collected the Raman spectra of the gelatin matrix, the silk, and the boundary of a cross-section of a bioFREE (Fig. S2A) and compared them based on the method by Vargas *et al.*[74] We did not identify chemical interactions at the interface *via* Raman spectroscopy and concluded that the interface between the gelatin matrix and the silk fiber are physical, primarily due to the saturation of the gelatin matrix between the silk fibers (Fig. S2B–D).

We next sought to understand the properties of gelatin-based actuators when pressurized. Fig. 5A depicts the change in water loss by weight percent over time at room temperature, and the maximum pressure held by bioFREEs at each time-point. The shaded area represents the standard deviation of the data, showing some variability in actuator performance before achieving a stable dry state. The data is smoothed with an exponential smoothing average with a coefficient of 0.6. The average maximum pressure that the bioFREE samples can withstand is marked along the curve. It is seen that the maximum pressure withstandable increases with a higher dehydration state.

To test the pressure limits of the 1 : 2 : 8 bioFREEs for each fiber-reinforcement type (silk fibroin +Fib, cotton +Fib, or no reinforcement −Fib), samples are measured and averaged at each water loss by weight percent interval (Fig. 5B). The data is smoothed with an exponential smoothing average with a coefficient of 0.6. Higher water weight loss corresponds to higher maximum pressures sustained by bioFREEs before failure, independent of reinforcement type. Both cotton and silk fibroin reinforced bioFREEs have similar performance at higher water weight loss amounts. At lower weight loss amounts, however, the saturation of the gelatin matrix into the silk fibers may be stronger, allowing silk to contribute more effectively to the composite strength.

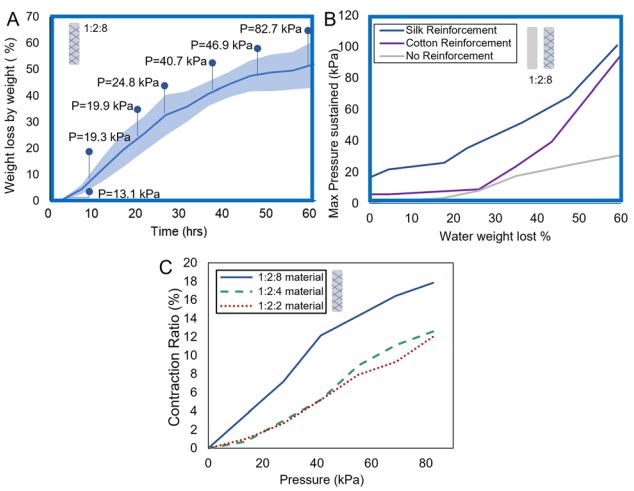

Fig. 5 Pressurizing bioFREEs at 21 °C and 50% RH. (A) Average maximum pressure for 1 : 2 : 8 bioFREEs is dependent on the dehydration water weight loss over time. The shaded region indicates the standard deviation among the samples (n = 3 batches). The data is smoothed with an exponential smoothing average (coefficient 0.6). (B) Average maximum pressure sustained based on the reinforcement type of bioFREEs at different dehydration weight loss percentages (n = 2 batches). The data is smoothed with an exponential smoothing average (coefficient 0.6). (C) Unloaded contraction ratio of the bioFREEs with different material compositions with increasing internal pressure. The red line indicates the maximum free contraction ratio of a silicone FREE at 17%, comparable to the 17.8% value of the 1 : 2 : 8 bioFREE.

Contraction ratio is a measure of actuator displacement for a given internal pressure. The unloaded contraction ratio of the silk-reinforced bioFREEs with increasing internal pressures is measured for different material compositions (Fig. 5C). The 1 : 2 : 8 material bioFREEs, however, have a noticeably higher free contraction ratio compared to 1 : 2 : 4 and 1 : 2 : 2 material bioFREEs since 1 : 2 : 8 becomes stiffer post-dehydration, transmitting stress more directly to the constraining fibers and axially contracting more efficiently rather than radially expanding. As observed in Fig. 4A, the 1 : 2 : 4 and 1 : 2 : 2 bioFREEs retain more water weight post-dehydration, making them more compliant and exhibiting less contraction. Thus, when the internal pressure causes deformation, some of the energy is dissipated within the material.

The 1 : 2 : 8 bioFREE has a free contraction of 16.4% at 82.7 kPa, a relatively high contraction per unit pressure when compared to synthetic materials. This makes gelatin FREEs especially attractive for low-power soft robotic systems, where energy efficiency and safe interaction with soft tissue are critical. This property is also ideal for low-pressure, portable/wearable systems where pressure-limited or compact form factor pumps must be used. Overall, the gelatin actuator demonstrates high-pressure efficiency and competitive contraction performance.

3.3. Force-based tests on bioFREEs

Next, we explored the loaded behavior of the bioFREEs. Blocked force tests measure the load capacity of a pneumatic soft actuator by isolating the actuator's force-generating capability when displacement is fixed.[75] The contraction ratio and the blocked force together determine the usefulness of the actuator for any given application by dictating its ability to generate both force and motion.[76] The blocked force is measured and averaged across three bioFREE samples for each material composition, following the procedure described in section 2.4. The changing geometrical parameters of the bioFREEs withstanding blocked forces due to internal pressures are seen in Fig. 6A.

The blocked force approaches 30 N when the internal pressure is 82.7 kPa for 0.5 cm diameter bioFREEs of all three material compositions (Fig. 6B). The blocked force for a bioFREE is typically maximally dependent on the resting fiber angle and minimally dependent on the elastomer material since the material deformation and strain are restricted,[77] there is, however, a nominally higher performance in the 1 : 2 : 8 material compared to the 1 : 2 : 4 and 1 : 2 : 2 materials. This is more apparent at higher pressures, where there is more bulging radial displacement and dependence on the material.

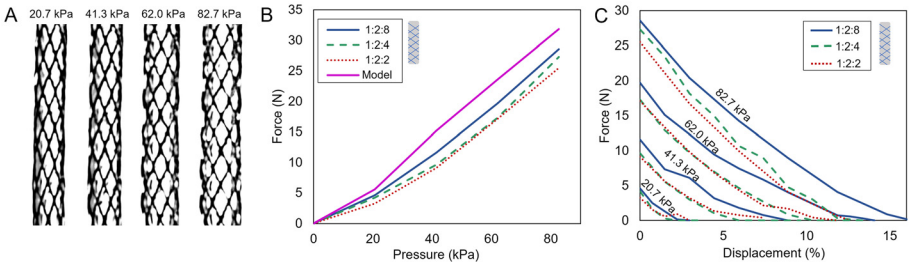

Fig. 6 Load tests on bioFREEs conducted in ambient conditions. (A) Images of 1 : 2 : 8 bioFREEs during testing show changes in radius (r) and twist angle (α) with increasing pressure. (B) Blocked force measurements of bioFREEs during stepwise pressurization for gelatin compositions 1 : 2 : 2, 1 : 2 : 4, and 1 : 2 : 8 compared to the theoretical model (eqn (1)). (C) Force exerted by contracting bioFREEs on negative displacement with varying internal pressures for the material compositions of 1 : 2 : 2, 1 : 2 : 4, and 1 : 2 : 8.

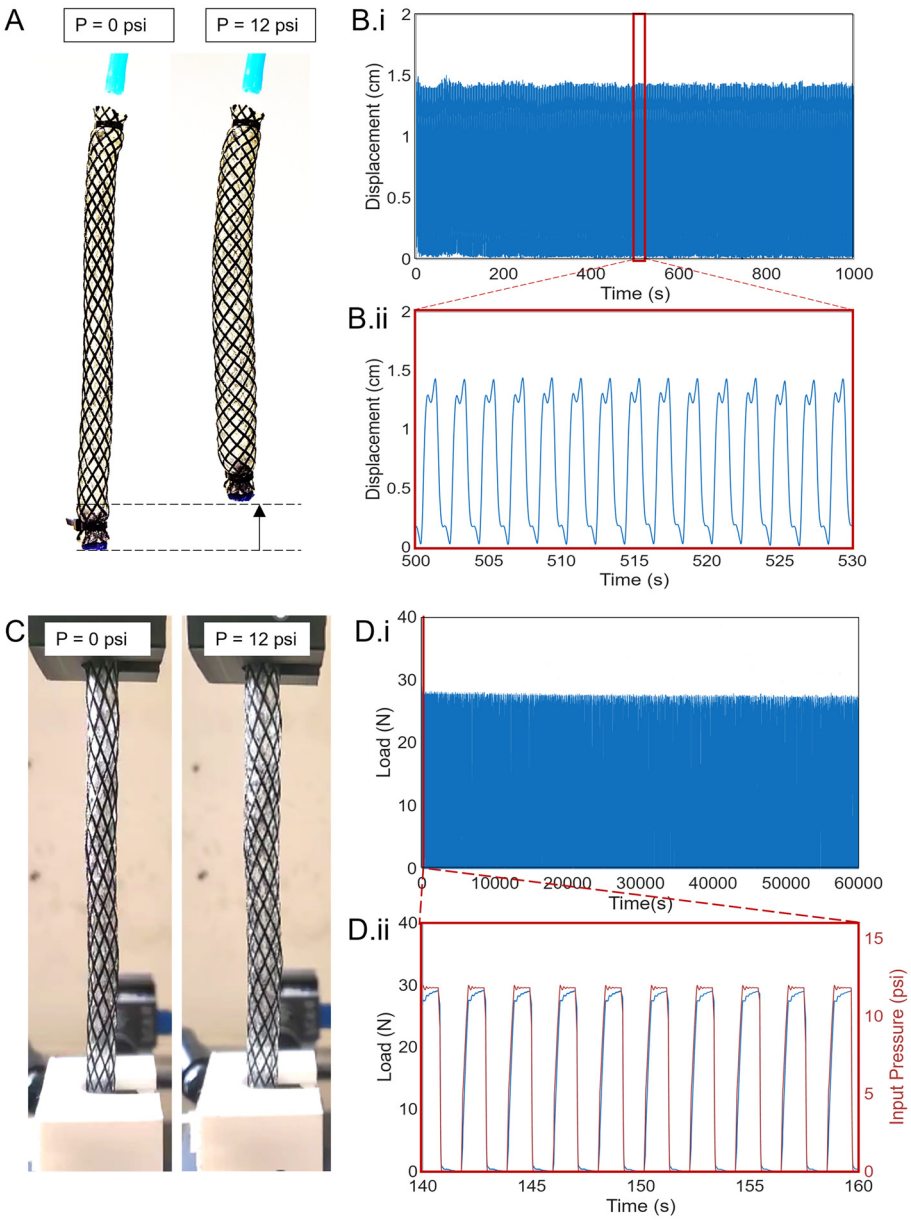

Fig. 7 Dynamic tests (A) cyclic pressurization to 40 000 cycles with 82.7 kPa of 1 : 2 : 8 bioFREEs (n = 3 bioFREEs). (B(i)) 1000 cycles plotted after 20 000 cycles run for sample 1. (B(ii)) Zoomed-in plot of B(i) for 15 cycles. (C) Cyclic loading to 40 000 cycles with 82.7 kPa of 1 : 2 : 8 bioFREE (n = 3 bioFREEs). (D(i)) 30 000 cycles of sample 1 (D(ii)) Zoomed in section from D(i) for 10 cycles (n = 3 bioFREEs).

The payload over the actuator weight is a ratio that acts as a metric for soft actuators. For the 1 : 2 : 8 bioFREEs with a weight of 5.5 g (0.054 N) that exert a blocked force of 28 N at an 82.7 kPa pressurization, ratio = payload (blocked force (N))/weight (N) = 28 N/0.054 N = 519. This lies on the high end for soft pneumatic actuators (including those made from non-biocompatible materials) that typically range from less than 30,[78,79] to sometimes over 1000.[80]

The blocked force for a FREE actuator has been modeled previously.[61,81–83] Blocked force depends on actuator parameters. The blocked force model here was originally derived by Kothera *et al.*,[61,82] with variables inner radius, r, wall thickness, t, fiber angle α measured with respect to its longitudinal axis, and Young's modulus, E_R.

$$F_{\text{blocked}} = \pi \overset{2}{\text{Pr}}\left(\frac{3\cos^2\alpha - 1}{\sin^2\alpha}\right) + \frac{2\pi r^2 E_R t}{\tan^2\alpha}\left(\frac{1}{r} - \frac{1}{r_0}\right) \quad (1)$$

The changing values for α and r were measured by image analysis captured during the blocked force testing Fig. 6A. There is a visible change in r and α with increasing pressures. For this reason, eqn (1) captures the experimental behavior of the 1 : 2 : 8 bioFREEs. The model's slope agrees with experimental data, but the error increases to 10% above ~20.7 kPa for the 1 : 2 : 8 FREEs. This error may be caused by fiber tautness or by pre-stress generated during dehydration shrinkage.

Similarly, tests are conducted to measure the steady-state force exerted by constrained bioFREEs when axially contracted to capture equilibrium steady-state force responses (Fig. 6C). Load capacities increase with increasing internal pressure. The strain-stiffening behavior of gelatin enhances the actuator's resistance to deformation under pressure, leading to a more gradual decrease in axial force decay as displacement increases compared to a linearly elastic material.

3.4. Dynamic testing

The contracting displacement of three bioFREE samples is tracked over 40 000 cycles of pressurizing (82.7 kPa) and venting for 1 second each (Fig. 7A). All three samples could run stable 40 000 cycles at a 1.5 cm displacement with no visible failures. 1000 cyclic pressurizations of sample 1 after 20 000 cycles are plotted in Fig. 7B(i). A moving average with a window of 10 is used to reduce the vibrational noise of the free-floating bioFREEs. Looking at a zoomed-in view of 15 cycles, the actuator relaxes first when vented, and then slower material relaxation brings the bioFREE back to its initial position (Fig. 7B(ii)).

We tested the cyclic blocked force exerted by the bioFREEs (L = 135 mm) across three samples when restrained between the MTS Criterion clamps and cyclically pressurized to 82.7 kPa (Fig. 7C). The test was run to 40 000 cycles with 1 second each for pressurizing and venting (30 000 cycles seen in Fig. 7D(i)). A zoomed-in view of 10 cycles shows the pressure signals along the load response (Fig. 7D(ii)). All three samples demonstrated a stable load of almost 30 N.

While the bioFREEs were tested for only up to 40 000 cycles for both the free contraction and loaded tests, the experiments depicted stable outputs with no failure or fatigue from the actuator or material, indicating that the actuators could continue to function for many more cycles. This demonstrates the actuator's durability and repeatability as a low-pressure wearable, biomedical, and agricultural use actuator, supporting gelatin as a viable, sustainable material for bioFREEs.

4. Conclusions

In this paper, we demonstrated the tunability of gelatin as an elastomer in bioFREE actuators. We demonstrated tunable material and component properties in response to dehydration state. There are some necessary considerations when utilizing these materials. The gelatin-glycerol formulation is hygroscopic and sensitive to humidity and temperature. The material can absorb water and swell in high humidity conditions, lowering the stiffness of the elastomer. In arid conditions, this material may continue to dehydrate and not maintain an intermediate level of dehydration (between 0 to 70%). Evolution of the gelatin properties with dehydration and plasticizer content can be further explored using FTIR or Raman analysis. Additionally, differential scanning calorimetry or thermogravimetric analysis can be used to understand the impact of material dehydration and temperature changes on the observed J-shaped mechanics and bioFREE load output. Although tunable dehydration states may be useful in some applications, such as in soil moisture sensing, there are ways to control water content for a consistent material stiffness. Some methods include building humidity-controlled chambers[84] around bioFREEs or applying moisture-barrier coatings to actuators after drying and dehydration. Electrospun polycaprolactone (PCL) is one such barrier material that has been used as a natural antimicrobial, oxygen, and water vapor barrier on gelatin constructs. Additonally, nanofiber coatings would not impede the sustainability of the actuator.[85] While biomaterials require new design criteria beyond those of synthetic chemsitries, these materials do open the design space to leverage new properties and applications in soft robotics.

Gelatin is a sustainable material that can be built into a protein-based bioFREE composite actuator when combined with silk fibroin reinforcement fibers. Our mechanical evaluation reveals that bioFREEs demonstrate functionality and durability to substitute common soft robotic materials like silicone or latex, with the added biomaterial properties. Gelatin bioFREEs with large dehydration can withstand maximum internal pressures and exert contraction ratios and blocked forces similar to those of silicone or latex FREEs. The passive properties of gelatin bioFREEs are tunable by harnessing gelatin dehydration to mimic the strain-stiffening seen in biological materials. This offers an opportunity to simulate the stretching of antagonistic ligaments and tendons in robotic joints.[86] BioFREE actuators have promising potential to help

expand soft robot applications in various medical and agricultural applications, including wearables, muscle mimics, implantables, harvesting, burrowing, and climbing robots. In summary, bioFREEs are a low cost method to test new types of sustainable and reliable robots for the future of this field.

Author contributions

S. E. and H. G. conceived of the experimental design and designed the study. B. K. advised on study design. S.E. fabricated the actuators, performed the experiments, compiled, and formatted the data. D. W. aided with sample fabrication and material tensile testing. D. W., J. R., and N. T. conducted serial actuator climbing demonstrations. S.E., H. G., and G. K. analyzed data. S. E. and H. G. wrote and edited the manuscript. All authors reviewed the final manuscript.

Conflicts of interest

There are no conflicts to declare.

Data availability

Data for this article are available at Illinois Data Bank, https://databank.illinois.edu/.

Spectroscopy methodology, results and plots are described in the supplementary document. See DOI: https://doi.org/10.1039/d5lp00370a.

Ref. 69–73, 87 and 88 are referenced in the SI document.

Acknowledgements

The authors thank the Bioengineering Department at the University of Illinois at Urbana-Champaign (UIUC). We also thank Dr David Ehrhardt and Dr Peter Kurath from the UIUC Advanced Materials Testing and Evaluation Laboratory (AMTEL) for their assistance with setting up the experiments and for the use of the facilities. Furthermore, we acknowledge the help from Dr Dianwen Zhang from the Microscopy Suite at the Beckman Institute for Advanced Science and Technology at UIUC.

This work was performed, in part, at the Center for Integrated Nanotechnologies, an Office of Science User Facility operated for the U.S. Department of Energy (DOE) Office of Science. Sandia National Laboratories is a multimission laboratory managed and operated by National Technology & Engineering Solutions of Sandia, LLC, a wholly owned subsidiary of Honeywell International, Inc., for the U.S. DOE's National Nuclear Security Administration under contract DE-NA-0003525. The views expressed in the article do not necessarily represent the views of the U.S. DOE or the United States Government.

References

1 H. Banerjee, Z. T. H. Tse and H. Ren, *Int. J. Robot. Autom.*, 2018, **33**, DOI: 10.2316/Journal.206.2018.1.206-4981.
2 G. Bao, H. Fang, L. Chen, Y. Wan, F. Xu, Q. Yang and L. Zhang, *Soft Rob.*, 2018, **5**, 229–241.
3 G. Alici, *MRS Adv.*, 2018, **3**, 1557–1568.
4 J. Xiong, J. Chen and P. S. Lee, *Adv. Mater.*, 2021, **33**, 2002640.
5 A. Pal, V. Restrepo, D. Goswami and R. V. Martinez, *Adv. Mater.*, 2021, **33**, 2006939.
6 T. Ashuri, A. Armani, R. Jalilzadeh Hamidi, T. Reasnor, S. Ahmadi and K. Iqbal, *Biomed. Eng. Lett.*, 2020, **10**, 369–385.
7 G. Chowdhary, M. Gazzola, G. Krishnan, C. Soman and S. Lovell, *Sustainability*, 2019, **11**, 6751.
8 S. M. G. Vidwath, P. Rohith, R. Dikshithaa, N. Nrusimha Suraj, R. G. Chittawadigi and M. Sambandham, in *Machines, Mechanism and Robotics*, ed. R. Kumar, V. S. Chauhan, M. Talha and H. Pathak, Springer Singapore, Singapore, 2022, pp. 1347–1353.
9 K. H. Petersen and R. F. Shepherd, *Robotic Systems and Autonomous Platforms*, Elsevier, 2019, pp. 61–84.
10 F. Hartmann, M. Baumgartner and M. Kaltenbrunner, *Adv. Mater.*, 2021, **33**, 2004413.
11 G. Giordano, S. P. Murali Babu and B. Mazzolai, *Front. Robot. AI*, 2023, **10**, 1116005.
12 J. W. Cohen Tervaert, *Mosaic of Autoimmunity*, Elsevier, 2019, pp. 297–305.
13 S. Bhatnagar and R. Kumari, *Annu. Res. Rev. Biol.*, 2013, **3**(4), 974–993.
14 M. Zare, E. R. Ghomi, P. D. Venkatraman and S. Ramakrishna, *J. Appl. Polym. Sci.*, 2021, **138**, 50969.
15 M. Kulkarni, S. Edward, T. Golecki, B. Kaehr and H. Golecki, *Soft Sci.*, 2025, **5**(12), DOI: 10.20517/ss.2023.51.
16 A. Firouzeh, M. Salerno and J. Paik, in 2015 IEEE/RSJ International Conference on Intelligent Robots and Systems (IROS), IEEE, Hamburg, Germany, 2015, pp. 1117–1124.
17 H. Su, X. Hou, X. Zhang, W. Qi, S. Cai, X. Xiong and J. Guo, *Actuators*, 2022, **11**, 92.
18 X. Zhang, M. Tian, T. Raza, H. Zhao, J. Wang, X. Du, X. Zhang and L. Qu, *Composites, Part B*, 2021, **223**, 109099.
19 N. Sholl and K. Mohseni, *Commun. Eng.*, 2024, **3**, 25.
20 G. Krishnan, J. Bishop-Moser, C. Kim and S. Kota, *J. Mech. Robot.*, 2015, **7**, 041014.
21 T. E. Pillsbury, C. S. Kothera and N. M. Wereley, *Bioinspiration Biomimetics*, 2015, **10**, 055006.
22 G. Krishnan, J. Bishop-Moser, C. Kim and S. Kota, in Volume 4: 36th Mechanisms and Robotics Conference, Parts A and B, American Society of Mechanical Engineers, Chicago, Illinois, USA, 2012, pp. 1089–1099.
23 M. Krieg and K. Mohseni, US11001681, 2021.
24 N. Thompson, X. Zhang, F. Ayala, E. T. Hsiao-Wecksler and G. Krishnan, in 2018 IEEE International Conference on

Robotics and Automation (ICRA), IEEE, Brisbane, QLD, 2018, pp. 1533–1538.
25 N. Thompson, A. Sinha and G. Krishnan, in 2019 International Conference on Robotics and Automation (ICRA), IEEE, Montreal, QC, Canada, 2019, pp. 570–576.
26 D. Trivedi, A. Lotfi and C. D. Rahn, *IEEE Trans. Robot.*, 2008, **24**, 773–780.
27 N. Kumar Uppalapati, B. Walt, A. Havens, A. Mahdian, G. Chowdhary and G. Krishnan, in *Robotics: Science and Systems XVI*, Robotics: Science and Systems Foundation, 2020.
28 L. F. Deravi, H. M. Golecki and K. K. Parker, *J. Chem. Biol. Interfaces*, 2013, **1**, 25–34.
29 H. Na, Y.-W. Kang, C. S. Park, S. Jung, H.-Y. Kim and J.-Y. Sun, *Science*, 2022, **376**, 301–307.
30 K. R. Stevens, N. J. Einerson, J. A. Burmania and W. J. Kao, *J. Biomater. Sci., Polym. Ed.*, 2002, **13**, 1353–1366.
31 T. Nagai, A. Kurita and J. Shintake, *Front. Robot. AI*, 2021, **8**, 760485.
32 S. Edward and H. M. Golecki, *Actuators*, 2023, **12**, 63.
33 C. Sundaram and A. Keenan, *Indian J. Urol.*, 2010, **26**, 374.
34 A. N. Sardesai, X. M. Segel, M. N. Baumholtz, Y. Chen, R. Sun, B. W. Schork, R. Buonocore, K. O. Wagner and H. M. Golecki, *MRS Adv.*, 2018, **3**, 3003–3009.
35 M. Baumgartner, F. Hartmann, M. Drack, D. Preninger, D. Wirthl, R. Gerstmayr, L. Lehner, G. Mao, R. Pruckner, S. Demchyshyn, L. Reiter, M. Strobel, T. Stockinger, D. Schiller, S. Kimeswenger, F. Greibich, G. Buchberger, E. Bradt, S. Hild, S. Bauer and M. Kaltenbrunner, *Nat. Mater.*, 2020, **19**, 1102–1109.
36 J. Shintake, H. Sonar, E. Piskarev, J. Paik and D. Floreano, in 2017 IEEE/RSJ International Conference on Intelligent Robots and Systems (IROS), IEEE, Vancouver, BC, 2017, pp. 6221–6226.
37 D. Hardman, T. George Thuruthel and F. Iida, *NPG Asia Mater.*, 2022, **14**, 11.
38 C. Wang, V. R. Puranam, S. Misra and V. K. Venkiteswaran, *IEEE Robot. Autom. Lett.*, 2022, **7**, 5795–5802.
39 L. Yang, J. Miao, G. Li, H. Ren, T. Zhang, D. Guo, Y. Tang, W. Shang and Y. Shen, *ACS Appl. Polym. Mater.*, 2022, **4**, 5431–5440.
40 J. Hughes and D. Rus, in 2020 3rd IEEE International Conference on Soft Robotics (RoboSoft), IEEE, New Haven, CT, USA, 2020, pp. 836–843.
41 Y. Yamada, *IEEE Robot. Autom. Lett.*, 2021, **6**, 3777–3784.
42 J. Liu, C.-K. Liu and E. Brown, *J. Am. Leather Chem. Assoc.*, 2017, **112**, 410–419.
43 Q. T. H. Shubhra, A. K. M. M. Alam, M. A. Khan, M. Saha, D. Saha, J. A. Khan and M. A. Quaiyyum, *Polym.-Plast. Technol. Eng.*, 2010, **49**, 983–990.
44 Q. T. H. Shubhra, A. K. M. M. Alam and M. D. H. Beg, *Mater. Lett.*, 2011, **65**, 333–336.
45 A. Heiden, D. Preninger, L. Lehner, M. Baumgartner, M. Drack, E. Woritzka, D. Schiller, R. Gerstmayr, F. Hartmann and M. Kaltenbrunner, *Sci. Robot.*, 2022, **7**, eabk2119.
46 H. Harris, A. Radecka, R. Malik, R. A. Pineda Guzman, J. Santoso, A. Bradshaw, M. McCain, M. Kersh and H. Golecki, in 2022 Design of Medical Devices Conference, American Society of Mechanical Engineers, Minneapolis, MN, USA, 2022, p. V001T05A004.
47 J. Nakayama, M. Horiki, K. Denno, K. Ogawa, H. Oka and K. Domen, *Prosthet. Orthot. Int.*, 2016, **40**, 142–146.
48 M. Schara, M. Zeng, B. Jumet and D. J. Preston, *Front. Robot. AI*, 2022, **9**, 1012862.
49 B. H. Shin, Y.-B. Bang, S.-W. Choi and S.-Y. Lee, in 2010 IEEE/ASME International Conference on Advanced Intelligent Mechatronics, IEEE, Montreal, QC, Canada, 2010, pp. 367–372.
50 N. D. Naclerio, A. Karsai, M. Murray-Cooper, Y. Ozkan-Aydin, E. Aydin, D. I. Goldman and E. W. Hawkes, *Sci. Robot.*, 2021, **6**, eabe2922.
51 E. Del Dottore, A. Mondini, D. Bray and B. Mazzolai, in *Biomimetic and Biohybrid Systems*, ed. F. Meder, A. Hunt, L. Margheri, A. Mura and B. Mazzolai, Springer Nature Switzerland, Cham, 2023, vol. 14157, pp. 184–196..
52 M. W. M. Tan, H. Wang, D. Gao, P. Huang and P. S. Lee, *Chem. Soc. Rev.*, 2024, **53**, 3485–3535.
53 J. E. Lee, Y.-C. Sun and H. E. Naguib, *RSC Appl. Polym.*, 2025, **3**, 767–792.
54 J. Hua, Q. Zhao and X. Du, *J. Mater. Chem. B*, 2025, **13**, 14660–14676.
55 C. You, W. Qin, Z. Yan, Z. Ren, J. Huang, J. Ii, W. Chang, W. He, K. Wen, S. Yin, X. Zhou and Z. Liu, *J. Mater. Chem. A*, 2021, **9**, 10240–10250.
56 Custom Collagen, Superclear Gelatin Transparent Edible Gelatin, https://customcollagenshop.com/products/super-clear-gelatin?_pos=1&_psq=super&_ss=e&_v=1.0.
57 Carolina, Glycerol, https://www.carolina.com/specialty-chemicals-d-l/glycerol/FAM_865530.pr.
58 Michaels, Silk thread, https://www.michaels.com/product/the-beadsmith-silk-498908726832791568.
59 Cotton thread, https://123stitch.com/item/Coats-Clark-Cotton-All-Purp-Thread-225yd-Purple-3690/S970-3690.
60 Master Airbrush, 1/5 HP Cool Runner II Dual Fan Tank Air Compressor Kit Model TC-326T, https://www.amazon.com/Master-Airbrush-Runner-Compressor-TC-326T/dp/B07ZQM6R83/.
61 G. Singh, C. Xiao, E. T. Hsiao-Wecksler and G. Krishnan, *Bioinspiration Biomimetics*, 2018, **13**, 036010.
62 G. Bradski and A. Kaehler, *OpenCV*, 2008, https://sourceforge.net/projects/opencvlibrary/.
63 D. A. Knopf and M. Ammann, *Atmos. Chem. Phys.*, 2021, **21**, 15725–15753.
64 A. Charkhesht, D. Lou, B. Sindle, C. Wen, S. Cheng and N. Q. Vinh, *J. Phys. Chem. B*, 2019, **123**, 8791–8799.
65 J. L. Nelson and R. A. Robergs, *Sports Med.*, 2007, **37**, 981–1000.
66 P. Bergo, I. C. F. Moraes and P. J. A. Sobral, *Food Hydrocolloids*, 2013, **32**, 412–415.
67 J. C. Case, E. L. White and R. K. Kramer, *Soft Rob.*, 2015, **2**, 80–87.

68 Ecoflex 30, https://www.smooth-on.com/products/ecoflex-00-30/.
69 Y. Ma, X. Feng, J. A. Rogers, Y. Huang and Y. Zhang, *Lab Chip*, 2017, **17**, 1689–1704.
70 M. Ibrahim, A. A. Mahmoud, O. Osman, M. Abd El-Aal and M. Eid, *Spectrochim. Acta, Part A*, 2011, **81**, 724–729.
71 A. De Ninno, A. Castellano and E. Giudice, *J. Phys.:Conf. Ser.*, 2013, **442**, 012031.
72 G. Pezzotti, *J. Raman Spectrosc.*, 2021, **52**, 2348–2443.
73 J. Romann, J.-C. Valmalette, V. Chevallier and A. Merlen, *J. Phys. Chem. C*, 2010, **114**, 10677–10682.
74 J. Vargas, R. Akrami, N. Marín-Alzate, S. M. Mesa, G. Idarraga, C. A. Isaza, L. Yang and J. M. Meza, *Microsc. Microanal.*, 2023, **29**, 1250–1252.
75 M. Lodeiro, M. Cain and M. Stewart, *NPL REPORT DEPC MPR 040*, 2005, 1–47.
76 X. Zhang and G. Krishnan, *J. Intell. Mater. Syst. Struct.*, 2018, **29**, 1139–1156.
77 J. Garbulinski, S. C. Balasankula and N. M. Wereley, *Actuators*, 2021, **10**, 26.
78 P. M. Khin, H. K. Yap, M. H. Ang and C.-H. Yeow, in *2017 IEEE/RSJ International Conference on Intelligent Robots and Systems (IROS)*, 2017, pp. 2744–2750.
79 H. Li, J. Yao, C. Wei, P. Zhou, Y. Xu and Y. Zhao, *Mech. Mach. Theory*, 2021, **158**, 104226.
80 S. Li, D. M. Vogt, D. Rus and R. J. Wood, *Proc. Natl. Acad. Sci. U. S. A.*, 2017, **114**, 13132–13137.
81 C.-P. Chou and B. Hannaford, *IEEE Trans. Robot. Automat.*, 1996, **12**, 90–102.
82 C. S. Kothera, M. Jangid, J. Sirohi and N. M. Wereley, *J. Mech. Des.*, 2009, **131**, 091010.
83 G. Singh and G. Krishnan, *Smart Mater. Struct.*, 2017, **26**, 065024.
84 K. Unger, M. Anzengruber and A. M. Coclite, *Polymers*, 2022, **14**, 3987.
85 K. Figueroa-Lopez, J. Castro-Mayorga, M. Andrade-Mahecha, L. Cabedo and J. Lagaron, *Nanomaterials*, 2018, **8**, 199.
86 S. Xiao, Y. Shao, B. Li and X.-Q. Feng, *J. Mech. Behav. Biomed. Mater.*, 2020, **112**, 104086.
87 O. K. Gasymov, A. Aydemirova, O. Alekperov, R. B. Aslanov, K. Khalilova, N. Gasimov, N. Mamedov, I. Mamedova, S. Babayev and N. Gasanov, *Phys. Status Solidi C*, 2015, **12**, 628–630.
88 W. T. Y. Tze, S. O'Neill, C. P. Tripp, D. Gardner and S. Shaler, *Wood Fiber Sci.*, 2007, **39**, 184–195.